



UNIVERSITATEA BABEŞ-BOLYAI
FACULTATEA DE BIOLOGIE ŞI GEOLOGIE

TEZĂ DE DOCTORAT

Datarea prin luminescenţă stimulată optic folosind cuarţ
pentru construirea cronologiilor absolute a ultimului
ciclu glaciatic înregistrat în depozitele de loess.

On the dating of the last glacial cycle in loess deposits
using quartz optically stimulated luminescence.

DANIELA CONSTANTIN

PROMOTER (COORDONATOR ŞTIINŢIFIC)
PROF. DR. VLAD AUREL CÔDREA

CLUJ-NAPOCA 2015

✓ The research discussed in the present thesis has been carried out at the Luminescence Dating Laboratory, Institute for Interdisciplinary Experimental Research, Babeş-Bolyai University in Cluj-Napoca, Romania. An extremely fruitful one-month study stay has been carried out at the Nordic Laboratory for Luminescence Dating, Denmark in April 2014.

✓ The Luminescence Dating Laboratory of Babeş-Bolyai University was funded through project PN II RU TE 3-2011-3-0062 (Ministry of Education and Scientific Research).

✓ Daniela Constantin was supported by the Sectoral Operational Programme for Human Resources Development 2007-2013, co-financed by the European Social Fund, under the project POSDRU/159/1.5/S/133391 – „Doctoral and postdoctoral excellence programs for training highly qualified human resources for research in the fields of Life Sciences, Environment and Earth”.

Contents

1	Introduction	3
1.1	Loess as archive of Quaternary climate changes	3
1.2	General information on luminescence dating of quartz.....	3
1.3	Age discrepancies reported by the first luminescence chronologies constructed on Romanian loess	5
1.4	Aim of this thesis and contents overview.....	7
2	Geological setting of the investigated loess sites	11
3	Establishing luminescence chronologies for loess deposits using different grain sizes of quartz	13
3.1	Sample preparation, instrumentation and measurement protocol.....	13
3.2	Annual dose determinations	16
3.3	Discrepancies in equivalent doses and OSL ages confirmed on Romanian, Serbian and Chinese loess.....	17
4	Fundamental investigations into the cause of the SAR OSL age discrepancies on different grains-sizes of quartz	34
4.1	Quartz luminescence response to a mixed alpha-beta field.....	34
4.2	Fundamental investigations of natural and laboratory generated SAR dose response curves for quartz OSL in the high dose range.....	36
5	Concluding remarks.....	42
	References.....	43

Keywords: optically stimulated luminescence (OSL); luminescence dating; quartz; loess; last glacial cycle; Danube basin; Chinese Loess Plateau

1 Introduction

1.1 Loess as archive of Quaternary climate changes

The last interglacial-glacial cycle has been characterized by a complex spectrum of orbital scale oscillations, comprising millennial scale climate shifts (colder stadials and warmer stadials) and even centennial to the interdecadal, interannual variations, has been recorded (**Dansgaard et al., 1993; Svensson, 2008; Rasmussen et al., 2014**). It is also the period during which modern humans developed and migrated and for which a substantial amount of proxy records (e.g. oxygen isotope, magnetic susceptibility) are available. Investigating such climate variations in detail plays a key role in understanding and predicting possible future climate changes, either natural or influenced by anthropogenic activities.

Loess-paleosol deposits cover approximately 10% of the earth surface and represent an important, high-resolution and quasi-continuous continental archive of Quaternary paleoclimates (**Figure 1**). The accepted paradigm is that dust deposition and thus loess formation is usually enhanced during glacial times, whereas pedogenic processes leading to soil development are stronger during warm-wet climates, specific to interglacial periods. However, providing reliable chronological framing for loess deposits that would allow for independent comparison with other records is still a problematic issue.

1.2 General information on luminescence dating of quartz

Luminescence dating is at present, the most applied method in establishing absolute chronologies for loess, which is generally assumed to be an ideal material for developing, testing, and applying luminescence techniques. The

optically stimulated luminescence is a radiometric dating method that has the potential of covering age intervals spanning from 10^2 years to 10^6 years. It relies on the properties of some mineral grains such as quartz, feldspars, calcite, etc., to store energy resulted from exposure to the environmental radiation field during their burial within deposits, and release it in the form of light upon stimulation with heat (thermoluminescence - TL) or with light (optically stimulated luminescence - OSL) ensuring that the latent luminescence signal is zeroed or reset. Such materials are called dosimeters and their use in retrospective dosimetry (dating) is based on the functional relationship between the burial time that is the amount of stored energy, and the intensity of the luminescence emitted when exposed to light or heat. The OSL age reflects the time elapsed since the last exposure to light of the buried mineral. In a rough manner, it represents the ratio between the total dose of radiation absorbed during mineral burial (palaeodose) and the rate at which the radiation dose was delivered (annual dose). To estimate the absorbed dose during burial, the emitted luminescence is translated into dose by use of the single-aliquot regenerative dose (SAR) protocol (**Murray and Wintle, 2000; Wintle and Murray, 2006**), by establishing the dose response of the quartz under investigation. Onto the dose response thus constructed the natural luminescence signal is interpolated in order to obtain the equivalent of the palaeodose accumulated during burial, termed equivalent dose (D_e). The annual dose is calculated in these studies based on the specific activities of natural isotopes from ^{238}U , ^{235}U , ^{232}Th series and ^{40}K determined by high-resolution gamma spectrometry. The annual dose cumulates contributions from alpha, beta, gamma, and cosmic radiation fields. The factors that influence the size of the annual dose are the water content of the sediment,

depth, altitude and latitude, as well as the nature of the bedrock and dated sediments.

Technological developments in the past years has resulted in significant improvements in the achievable precision and accuracy using luminescence dating technique; this method is now considered one of the most important chronometers in the study of the late Quaternary (**Wintle, 2008**). At the same time, dating applications recently performed on Romanian loess by the application of optically stimulated luminescence on quartz lead to unexpected results.

1.3 Age discrepancies reported by the first luminescence chronologies constructed on Romanian loess

A first study has reported optically stimulated luminescence (OSL) ages for the loess sequence near Mircea-Vodă (Dobrogea, SE Romania) using silt-sized (4-11 μ m) quartz as dosimeter (**Timar et al., 2010**). An internally consistent set of optical ages was obtained; however, a comparison of these ages with a magnetic time-depth model based on magnetic susceptibility measurements suggested a systematic underestimation beyond the penultimate glacial period (the SAR OSL ages of the three samples below the S1 soil were interpreted as age underestimates). Interestingly, the OSL signals from these samples did not indicate any odd characteristics. It was concluded that optical dating of fine-grained quartz can be used to establish a reliable chronology for Romanian loess up to ~70 ka corresponding to an equivalent dose of ~ 200 Gy. Such a behaviour is consistent with results from old (>70 ka) Chinese loess (**Buylaert et al., 2007**), and with the more general suggestion that SAR may underestimate the true age in the older age range (**Murray et al., 2007**;

Lowick et al., 2010a; Lowick et al., 2010b; Lowick and Preusser, 2011). Thus, apparently reliable OSL laboratory measurement procedure does not necessarily guarantee an accurate determination of the true burial dose. A subsequent study of coarse-grained (63-90 μm) quartz extracted from the same section (**Timar-Gabor et al., 2011**) revealed that equivalent doses obtained for coarse quartz grains were systematically larger than those for the fine grains; the observed difference was too high to be explained by partial bleaching or microdosimetric effects. Furthermore, both quartz fractions passed the procedural tests of the single-aliquot regenerative-dose (SAR) and yielded an internally consistent set of optical ages.

Timar-Gabor et al. (2012) investigated into the shape of the dose response for the two grain size fractions in the high dose region 5-10 kGy and two additional issues of general importance to SAR emerged. Firstly the natural signal of an infinitely old sample was found not to be in saturation, perhaps implying that the dose response measured in the laboratory may not simulate trapped charge growth during burial. Secondly, it was observed that the dose response curve for coarse grains (63-90 μm) is very different from fine grains (4-11 μm), the latter saturating at much higher doses. A similar observation has also been made by **Constantin et al. (2012)** where fine grains (4-11 μm) and coarse grains of different sizes (63-90, 90-125, 125-180 μm) were compared in a Căciulatești site (SW Romania). This is mostly intriguing in correlation to the fact that the fine fraction underestimates the true ages sooner than the coarse one. Also it is important to note that the values obtained for the saturation characteristics for the fine quartz fraction are very similar to the values reported by other international studies (e.g. **Lowick et al., 2010b**) in their work on fine material, while the saturation characteristic doses obtained

in this study for coarse grained quartz are close to the values previously reported by others on coarse material from other locations (**Murray et al., 2007; Pawley et al., 2010**).

1.4 Aim of this thesis and contents overview

This thesis relies on the 5 articles I have authored and co-authored during the 3 years of my PhD studies. It also presents results obtained on Chinese loess which will be the subject of future publications. Outlined below is the overall thesis structure and the motivations for each of the following chapters are described.

Part 1 comprises **Chapters 2 to 5**. High-resolution optically stimulated luminescence chronologies are constructed for the Last Glacial cycle employing the single aliquot regenerative dose (SAR) protocol applied to silt (4-11 μm) and fine sand (63-90 μm) quartz. The four loess sections investigated here were selected as to provide a regional and even transcontinental perspective over the two issues revealed in the Mircea-Vodă site: (i) the age underestimations of fine and coarse quartz from older samples, as discussed above, and (ii) the different dose response characteristics of the two grain sizes of quartz.

Chapter 2 reports fine and coarse quartz high-resolution SAR-OSL chronologies for the L1, S1 and L2 units of the loess-palaeosol profile from Costinești in Dobrogea, southeastern Romania to test whether the age discrepancy yielded by the different quartz grain-sizes in Mircea-Vodă is a local feature.

It was previously demonstrated (**Buggle et al., 2008**) that the geochemical composition of the loess from Mircea-Vodă (SE Romania) and the Serbian loess share a major component derived from the Danube alluvium. However, loess particles from Dobrogea indicate a significant contribution of a second loess source, probably the glaciofluvial sediments in Ukraine, to which variable contributions from local sand dunes fields can be considered. As such, the area of study is extended to more westerly loess deposits with components originating from different sources: Lunca site in western Romania (Lower Danube basin) and Orlovat site in Serbia (Carpathian basin). As such, in **Chapters 2** and **3** it is examined whether the source of the quartz might be the cause of the above mentioned issues.

The similarity of southeastern European loess material characteristics, and its environmental origins, enables comparison and stratigraphic correlation between these plateau deposits and those of central China (**Stevens et al., 2011; Marković et al., 2015**). The Chinese Loess Plateau in north-central China potentially contains ~25 Ma of loess accumulation and is the longest and most continuous dust archive on the planet (**Liu and Ding, 1998; Guo et al., 2001**). Through the multitude of available proxies, it has provided fundamental insights into the Quaternary climate oscillations. Yet, the absolute chronologies based on luminescence dating of quartz that should support such palaeoclimate models are rather scarce and their reliability is usually restricted to the last glacial period or even later, based on the choice of the method or mineral used. In the light of the reported issues on the southeastern European loess, in **Chapter 5** the luminescence dating method is applied on two grain-sizes of quartz extracted from the famous Xifeng loess section (**Kukla, 1987; Stevens et al., 2007**). Through comparison of the

luminescence properties of quartz, it is evaluated whether the age discrepancy of the two quartz grain-sizes as well as their different pattern of OSL signal growth represents a worldwide feature.

Part 2 of this thesis comprises methodological investigation into the cause of the OSL age discrepancies presented in **Chapters 6-7**.

Since a major difference in coarse- and fine-grained quartz dating lies in the alpha irradiation history, in **Chapter 6** it is investigated whether the alpha dose experienced by fine grains over geological cycles of irradiation and bleaching have an effect on the saturation characteristics of the laboratory dose response.

In **Chapter 7** a step further is taken into understanding the disturbing observations of Timar-Gabor et al. (2012) on laboratory dose responses that do not reproduce the growth of the OSL signal with dose in nature. On Romanian, Serbian and Chinese quartz samples, CW-OSL and pulsed OSL average laboratory dose response curves are constructed up to very high doses to determine and compare their saturation characteristics. Additionally, the effect of previous irradiation, bleaching or thermal treatments on the obtained laboratory saturation characteristics is also probed. Time resolved luminescence is applied on these quartz extracts in order (i) to test whether the observed luminescence growth in laboratory is a characteristic of quartz rather than an artefact caused by feldspar contamination, and (ii) to determine whether luminescent recombination occurs at different centres at large doses. Natural growth curves are constructed on two Romanian loess sites based on the data derived from magnetic susceptibility time-depth model and compared to average laboratory growth curves. Unfortunately, the lack of an independent

age model hindered the construction of natural growth curves for the Xifeng site studied in this thesis. Thus, the results obtained on Romanian loess were compared to the only natural dose response available from another type section of the Chinese Loess Plateau (**Chapot et al., 2012**). Additional experiments on Romanian and Chinese quartz are carried out in order to test whether SAR protocol can accurately recover high natural or laboratory doses.

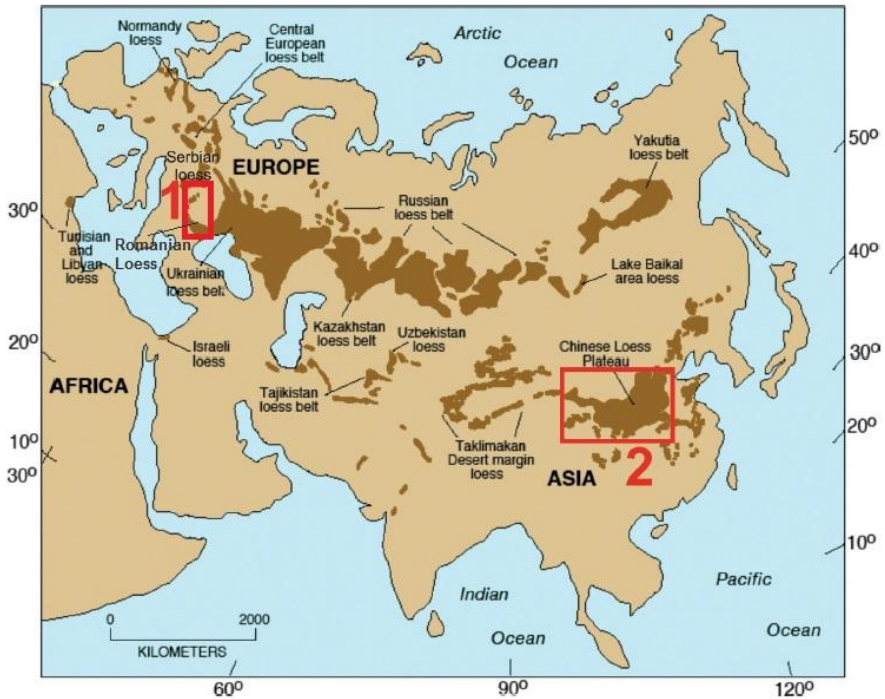


Figure 1 Distribution of the loess sediments modified from **Muhs (2007)**; **Marković et al. (2012)**): 1. Romanian and Serbian loess; 2. Chinese Loess Plateau.

2 Geological setting of the investigated loess sites

Direct stratigraphic correlation of the loess deposits from the Middle and Lower Danube basin to those of central Chinese Loess Plateau was reported by **Marković et al. (2015)**. Therefore, a stratigraphic labelling scheme following the Chinese loess stratigraphic model (**Kukla and An, 1989**) is applied to all investigated sections in this thesis for ease of intercomparison. The loess and palaeosol stratigraphic units are designated as L and S and are numbered in order of increasing age. In all sites investigated, except Lunca, the sampling strategy covered the stratigraphic units from the upper part of the penultimate loess layer upwardly.

From a structural viewpoint, the studied Romanian loess sequences are located inside the Moesian Platform. The Costinești site is situated in South Dobrogea, which is a distinct unit of this platform that now can be directly observed on surface in Romania between Capidava-Ovidiu fault and the Bulgarian border, whereas the Lunca site is located inside the Western Moesian Platform.

The site from Costinești represents a cliff-exposure along the Black Sea shore (43, 97° N; 28, 65° S; Dobrogea, southeastern Romania). The Quaternary loess directly overlies Sarmatian limestone and consists of approximately 12.5 m-thick deposits comprising six loess-palaeosol alternations (L1 to L6 interbedding S1 to S5). Palaeosols S1 and S2 are chernozems, whereas S3 to S6 are brown-reddish forest soils. Primary remanent magnetisation measurements constrain the age of this Costinești village section to a maximum of 730 ka (**Ghenea and Rădan, 1993**).

In southwestern Romania, vertical exposures of typical loess deposits measuring tens of meters in thickness dominate the alluvial plain along the left

side of the Olt and Danube valley. The site of Lunca (43°50'55" N, 24°45'56"E) is located in southern Wallachian Plain, on the left bank of the Olt River, approximately 15 km north to its confluence with the Danube River. This section appears as an ~36-metres-deep ravine cut and it has been previously the subject of rock magnetic susceptibility measurements (**Necula, 2006**) that identified at least 6 loess-palaeosol alternations.

The investigated loess–palaeosol sequence of Orlovat located at the north-eastern margin of the Vojvodina loess plateau, which from a structural perspective is located inside the Pannonian Basin. The investigated profile is exposed in a brickyard (45°15' N, 20°35' E), in the central part of the Tamiš loess plateau in contact with the Tamiš river valley, northern Serbia.

The loess deposits in the vicinity of the Xifeng city are regarded as “type loess sections” of the central Chinese Loess Plateau, which from a structural viewpoint is located within the Ordos basin (northern China craton). Complete sections display 33 loess-palaeosol successions reaching thicknesses up to 300 meters and are commonly underlain by well weathered red silt clay sediment, informally named the Red Clay formation. Their contact has been paleomagnetically dated at about ~2.4 Ma. The Red Clays in Xifeng date from the Gilbert and Gauss magnetic epochs (Late Pliocene) and their basal sand and gravel rests unconformably on pre-Tertiary bedrock (**Kukla, 1987**). New basal dates from ‘Red Clay’ sediments on the Chinese Loess plateau indicate onset of aeolian dust accumulation at about 8 Ma ago and were interpreted as signalling an environmental response to a major phase of Himalaya-Tibetan plateau uplift about 9-8 Ma ago (**An et al., 2001**). In the present study a fresh loess exposure has been sampled for OSL dating, other than the loess profiles studied by **Kukla (1987)** or by **Stevens (2006); (2007)**. Sampling strategy was

based on field observations and magnetic susceptibility variations down the section along three separate but consecutive profiles reaching 17 m.

3 Establishing luminescence chronologies for loess deposits using different grain sizes of quartz

In Chapters 2 to 5 high-resolution absolute chronologies for the last glacial cycle recorded in the loess-palaeosol successions from the Danube basin in southeastern Europe and the Chinese Loess Plateau are presented. The luminescence measurements were carried out on fine (4-11 μm) and coarse (4-11 μm) quartz to test whether the OSL age discrepancies observed in Mircea-Vodă site represent a worldwide spread phenomenon. As an independent age control magnetic susceptibility time-depth models are constructed for Costinești and Lunca sections.

3.1 Sample preparation, instrumentation and measurement protocol

Samples were collected by hammering stainless-steel cylinders onto freshly cleaned loess exposures at different intervals for each of the investigated profiles (see **Table 1-4**). The material at each end of cylinder was extracted for high resolution gamma spectrometry and water content estimations.

The core material is treated with diluted HCl (10%) to remove carbonates, and then repeatedly washed with distilled water. To remove organic materials, 10%, respectively 30% H_2O_2 is added and then samples are subsequently washed several times with distilled water. Following this pre-treatment, wet sieving is performed using the 90 μm and 63 μm sieve meshes. After sieving,

the left fraction consists of an undifferentiated mixture of minerals, including quartz, feldspars and heavy minerals. These minerals have slightly different densities and for coarse grain dating they can be separated in suspension using heavy liquids (sodium metatungstate $\text{Na}_6[\text{H}_2\text{W}_{12}\text{O}_{40}] \times \text{H}_2\text{O}$ (a heavy inorganic salt) with distilled water. First the polymineral sample is suspended in a solution with a density of 2.62 g/cm^3 . This enables the separation of quartz and plagioclase grains from the lighter minerals such as clay, potassium and sodium feldspars. Subsequently, the mineral grains are suspended in a solution with a density of 2.75 g/cm^3 . In this case, quartz and plagioclase feldspars will float while heavy minerals such as zircons and apatite will sink. The floating fraction is kept, washed and dried. Quartz can no longer be separated from plagioclase by means of difference in density. Therefore, a treatment with 40% hydrofluoric acid (40 min) is performed. The feldspars are less chemically resistant and are dissolved. The etching also removes the outer surface of the quartz grains, which reduces the external alpha particle contribution to these grains to a negligible level. A wash with diluted HCl is applied after etching to remove any precipitated fluorides. This is followed by repeated washing with distilled water and drying. Finally the product is sieved again to obtain the desired grain size. To extract fine grains, the fraction less than $11 \mu\text{m}$ is isolated by settling in Atterberg cylinders according to Stokes' law. For removal of feldspars and obtaining quartz fine grained samples attack with 35 % hydrofluorosilicic acid (H_2SiF_6) (10 days) is performed. For measurement coarse quartz grains are mounted on stainless steel disks using silicon oil as adhesive. Quartz fine grains are deposited on aluminum disks by acetone suspension. The absence of a significant infrared stimulated luminescence response at $60 \text{ }^\circ\text{C}$ to a large regenerative β -dose confirmed the

purity of the quartz extracts. The purity of each aliquot analysed was further monitored by IR depletion tests (**Duller, 2003**) and by observing the 110 °C TL signals during preheating.

All continuous wave optically stimulated luminescence measurements (CW-OSL) were made in Cluj Luminescence Dating Laboratory with a Risø TL/OSL DA-20 reader equipped with blue light emitting diodes (LEDs) emitting at 470 ± 30 nm and IR LEDs emitting at 870 nm; luminescence signals were observed through a 7.5 mm thick Hoya U-340 UV filter. Irradiations have been carried out using a ^{90}Sr - ^{90}Y beta source, calibrated using quartz supplied by Risø National Laboratory. The OSL signal was collected in time intervals of 0.154 s. All samples have been analysed in a SAR protocol (**Murray and Wintle, 2000, 2003**). The OSL signal used for analysis was that obtained for the first 0.308 s of the decay curve minus a background derived from the signal measured between 2.464 and 3.080 s, as had been used in previous studies on Romanian loess (**Timar et al., 2010; Timar-Gabor et al., 2011**).

Natural and regenerated signals were measured after a preheat of 10 s at 220°C unless otherwise stated; the response to the test dose (16 Gy) was measured after a cutheat to 180°C. The value of the test dose was kept constant through all measurements for both grain sizes of quartz. After the measurement of the response to the test dose, a high-temperature bleach was performed by stimulating with the blue diodes for 40 s at 280 °C.

Time resolved optically stimulated luminescence (TR-OSL) experiments have been carried out in Risø National Laboratory on a Risø TL/OSL-20 equipped with an integrated pulsing option to control the LEDs, and a Photon Timer

attachment to record the TR-OSL. All time resolved optically stimulated luminescence experiments have been carried out using the same measurement parameters previously used in CW-OSL. For stimulating and recording the TR-OSL signals the total measurement time was set to 100s, with a pulse period of 500 μ s consisting of an on time of 50 μ s and an off time of 450 μ s; this can be translated to a net stimulation period equivalent to 10s in CW-OSL. A total of 500 data points were used for data collection in pulsed stimulation out of which the first and the last five channels were dead channels. Measurement of dose response curves using pulsed optically stimulated luminescence measurements have been specially designed in order to reproduce the CW-OSL measurements conditions as closely as possible, and to minimise any possible feldspar contamination to quartz, by: (i) selection of an on time of 50 μ s (ii) gating the photomultiplier for counting only during the off period; (iii) ignoring the first 4 μ s during the off time in TR-OSL OSL data analysis (**Ankjærgaard et al., 2010**).

The specific activities of radionuclides of interest for dose rate determination were obtained through high-resolution gamma spectrometry using an ORTEC hyperpure germanium detector having the following characteristics: active volume of 181 cm³, 0.878 keV FWHM at 5.9 keV, 1.92 keV FWHM and 34.2 % relative efficiency at 1332.5 keV, calibrated in efficiency using International Atomic Energy Agency standards.

3.2 Annual dose determinations

High-resolution gamma spectrometry was used to derive the concentrations from ²³⁸U, ²³²Th, ⁴⁰K in our samples. The dose rates were calculated using the conversion factors tabulated by **Adamiec and Aitken (1998)**. Total annual

dose rates include a small contribution from cosmic radiation evaluated according to **Prescott and Hutton (1994)**. A time-averaged water content of $10 \pm 2.5\%$ was used to correct the alpha, beta and gamma contributions for the effect of moisture. The beta attenuation and etching factors for 63-90 μm fraction are 0.94 ± 0.05 (**Aitken, 1985**). An a -value of 0.04 ± 0.02 was adopted to allow for the lower efficiency of alpha radiation in inducing luminescence in fine grains (**Rees-Jones, 1995**).

3.3 Discrepancies in equivalent doses and OSL ages confirmed on Romanian, Serbian and Chinese loess

All samples investigated displayed bright and rapidly decaying OSL signals that are independent of the given irradiation dose and insets in Figure 2 show representative example. The performance of the SAR protocol applied for all samples was tested in terms of recycling, IR depletion and recuperation. Recycling ratios don't exceed the 10% deviation from unity and the growth curve passes close to origin. This general good behaviour is representative for every sample investigated. The laboratory dose response is fitted by a sum of two saturating exponential functions:

$$I(D) = I_0 + A \left(1 - e^{-\frac{D}{D_{01}}} \right) + B \left(1 - e^{-\frac{D}{D_{02}}} \right)$$

Where $I(D)$ represents the corrected OSL signal levels induced by the given dose D and I_0 stands for the maximum luminescence intensity, D_{01} and D_{02} indicate the characteristics doses for the onset of saturation in each component and A , B represent the corrected luminescence levels corresponding to D_{01} and D_{02} respectively. The OSL signal yielded by fine grains grows to higher doses compared to coarse grains. In the example given and for all samples, the

corrected natural OSL signal is interpolated well below the laboratory saturation level of the growth curve.

Dose recovery tests have been carried out on every sample according to the methodology outlined by **Murray and Wintle (2003)**. The given dose was chosen to be as close as possible to the estimated equivalent dose and at least three aliquots have been used for each test. **Figure 3** presents the representative results obtained for fine grains (**panel a**) alongside with the results obtained on coarse grains (**panel b**). It can be noted that for all samples laboratory given doses can be measured both accurately and precisely.

Equivalent doses have been determined as the arithmetic mean of individual aliquots results. **Tables 1-4** summarize the relevant information to equivalent dose measurement and age determination on all samples investigated in this thesis. As previously reported for the Mircea-Vodă site, beyond 100 Gy, the fine quartz equivalent doses are systematically lower compared to those of coarse quartz; contrary to the dosimetric expectation, the values derived from the coarse quartz are systematically higher than the values obtained for fine quartz.

One possible cause of concern is related to a thermal instability of the OSL signal sampled from the fine fraction. This could be caused either by contamination of the signal with an unstable medium OSL component (see e.g. (**Choi et al., 2003; Steffen et al., 2009**)), or by a thermal instability of the fast OSL component itself (**Fan et al., 2011**). This has been tested on all sample sets using preheat plateau tests (**Figure 4 a**) and high resolution pulse annealing experiments for both natural and regenerated signals (**Figure 4. b**).

For all loess sections scrutinized, there is no dependency of the measured equivalent dose on preheat temperature and the three datasets obtained in pulse anneal experiments (natural, regenerated and calibration quartz) suggest that the stability of the fast component for both grain sizes is the same, therefore, the long term stability of the signal should not be a problem.

Potential contamination with feldspars that cannot be detected through IR depletion ratio tests was ensured by time-resolved optically stimulated luminescence investigations that can discriminate quartz from feldspar (**Ankjærgaard et al., 2010**). TR-OSL investigations on fine and coarse quartz from samples CST 3, LCA 26, ORL 4, XF 13 and XF 175 are reported. On all samples investigated the signal display a slow decay during the off-time, typical of quartz. The shape and amplitude of the signal is not sensitive to prior IR stimulation. **Figure 5** shows a representative time-resolved luminescence signals induced by different beta doses for a coarse quartz aliquot of sample LCA 26. Pulsed OSL growth curves were constructed and the equivalent doses obtained using pulsed OSL on samples CST 3, ORL 4, XF 13 and XF 175 which are in good agreement with the CW-OSL equivalent doses (data not shown).

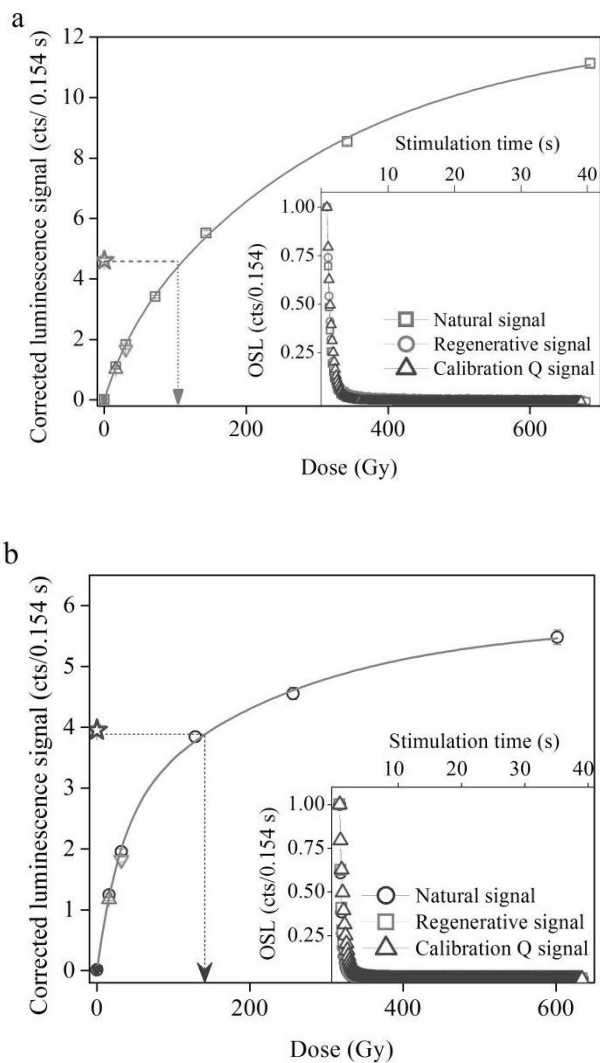


Figure 2 Representative SAR-OSL growth-curves for an aliquot of (a) fine quartz extracted from sample LCA 15 represented with open squares and (b) coarse quartz extracted from sample LCA 24 given with open circles. Recuperation values are indicated with filled (a) square and (b) circle; recycling and IR depletion dose points are shown as point-up and point-down triangles, respectively. The sensitivity corrected natural luminescence signal is represented as a star and the obtained equivalent dose is indicated by arrow. Insets show the natural and regenerated signal decay compared to the calibration quartz signal decay.

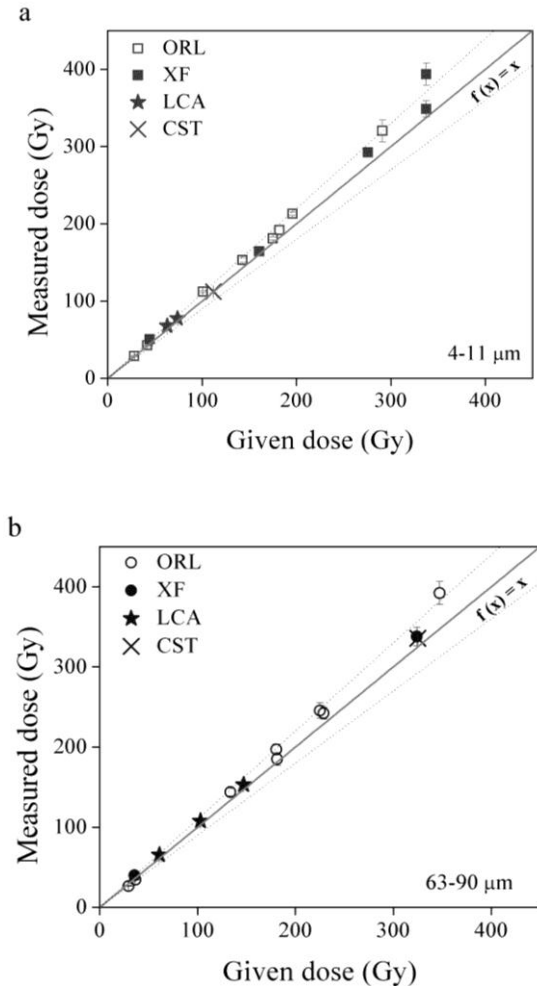


Figure 3 Summary of dose recovery data for all fine (4-11 μm) grains (panel a) and coarse (63-90 μm) grains (panel b) samples from all the investigated sections. Natural aliquots were bleached twice for 100 s at room temperature using the blue light emitting diodes; the two bleaching treatments were separated by a 10 ks pause. The aliquots were then given a known dose chosen to be equal to the estimated equivalent dose, and measured using the SAR protocol. The solid line (eye guide) represents the 1:1 relation; the dotted lines (eye guide) bracket a 10% deviation from unity.

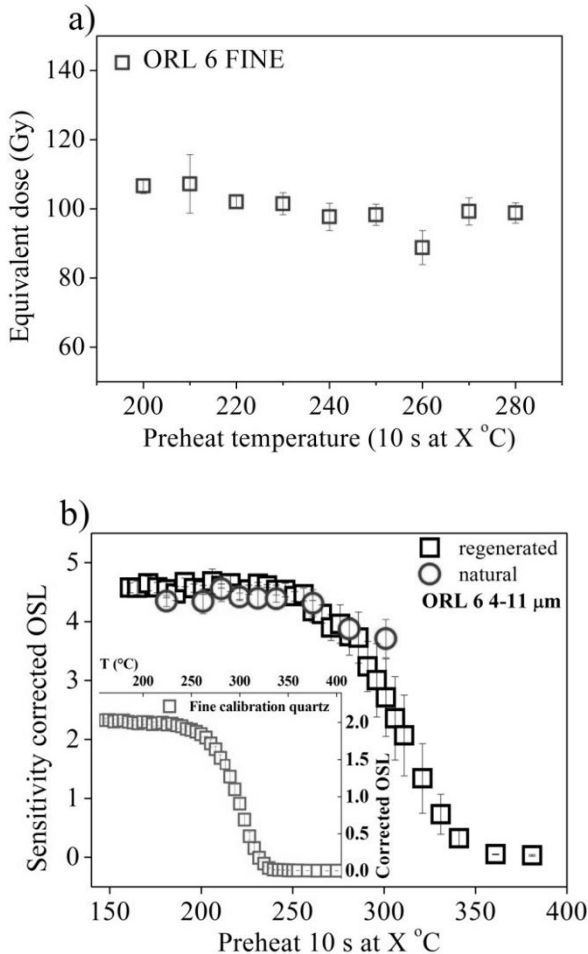


Figure 4 (a) Representative results of the equivalent dose preheat plateau test performance. **(b)** High resolution pulse anneal test for natural and regenerated signal. For natural signals each data point presents the average value obtained on three aliquots of the ratio between the natural signal measured after different preheat (10 s) temperatures and a 16 Gy test dose signal. In the case of regenerated signals three fresh aliquots have been bleached, given a dose approximately equal to the equivalent dose, the OSL signal being measured at 125 °C following different preheat (10 s) temperatures, each value being normalized to the response to a constant test dose of 16 Gy (cutheat to 180°). The insert presents data obtained using Risø calibration quartz.

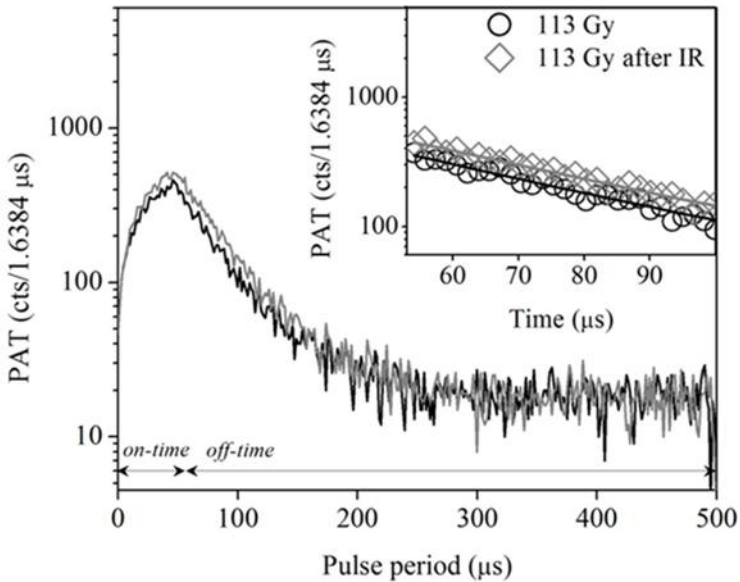


Figure 5 Photon arrival time distribution for 63-90 μm quartz from sample LCA 26. The TR-OSL has been recorded during the pulsing period (500 μs) at a resolution of 1.6384 μs . The black solid line represents the response to 113 Gy. The grey solid line represents the response to the same dose but with a prior IR bleach applied. The graph shows summed data in 100 s of blue LED's stimulation at 125 $^{\circ}\text{C}$. Insert: close-up of photon arrival time distribution during the off-time (except the first 4 μs), showing data from the 54 – 100 μs ; the solid lines in insert represent the best fit of the data - a single exponential decay plus a constant. Please note the logarithmic scale.

For all the investigated sections from Romania, Serbia and China (except Costinești where only De 's > 100 Gy were obtained due to the sampling limitations) it was found that the OSL ages on the different grain-sizes agree for those samples with De 's < ~100 Gy (~20–30 ka). For higher equivalent doses and hence older samples there is a marked discrepancy between the ages obtained on fine and coarse quartz. As sustained by stratigraphic observations as well as by the comparison to the available magnetic susceptibility age-depth model, the OSL chronology provided by fine quartz tends to underestimate sooner than the coarse quartz the true burial age.

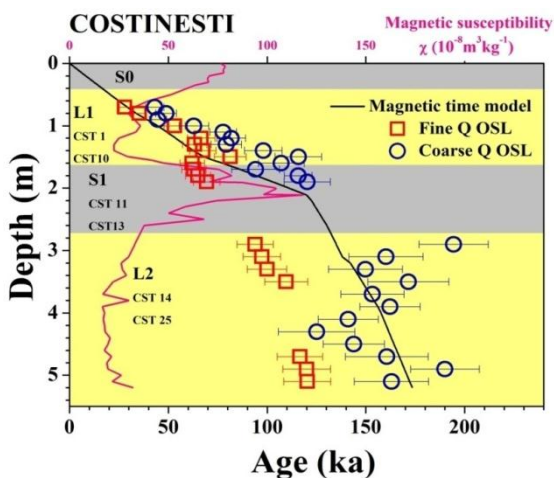
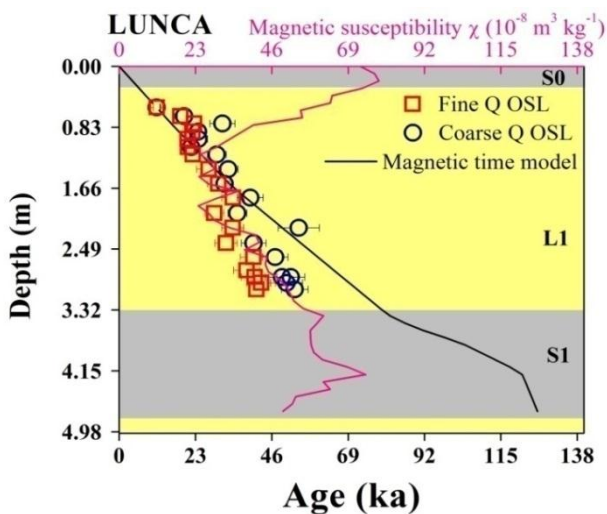


Figure 6 Optical ages on fine quartz (open squares, 1σ total uncertainties) and coarse quartz (open circles, 1σ total uncertainties) plotted against sampling depth. The magnetic time-depth model represented as solid line is used for comparison while the magnetic susceptibility variation measured along the investigated profile is indicated by a dashed line. The loess and palaeosol stratigraphic units are designated as L and S and are numbered in order of increasing age.

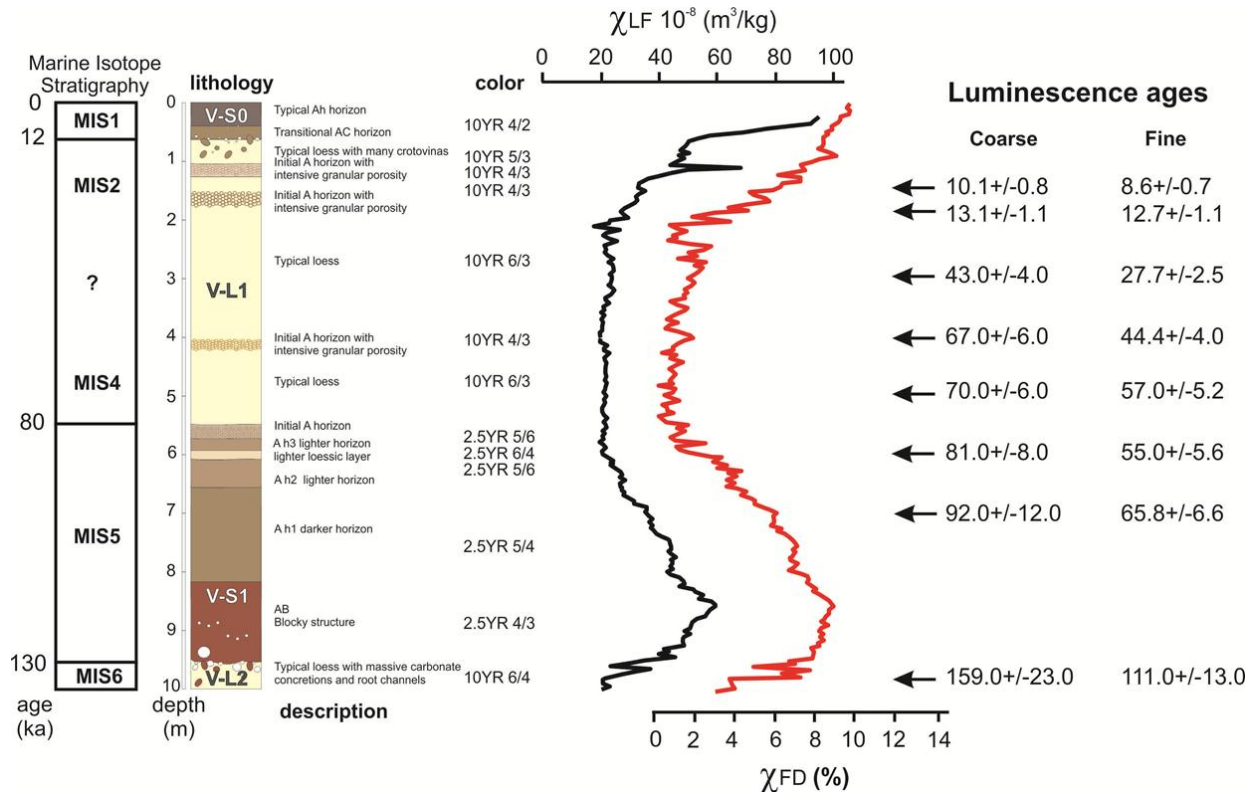


Figure 7 Orlovat loess site. Stratigraphic column, description, sediment colour and magnetic properties of the investigated section compared with MIS (Martinson et al., 1987) and luminescence age results. The location of the luminescence samples is indicated by arrows.

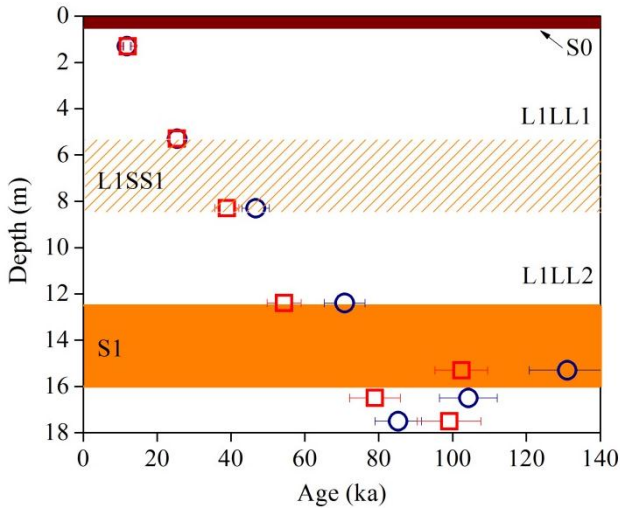


Figure 8 The Xifeng site, central Chinese Loess Plateau China. SAR-OSL ages on fine (open squares, 1σ total uncertainties) and coarse (open circles, 1σ total uncertainties) quartz are plotted against sampling depth. Last glacial loess is labeled with L1 while the modern soil and the last interglacial units are given with S0 and S1 respectively. L1SS1 indicated the weakly developed palaeosol from the middle pleniglacial and its formation can be correlated to MIS 3.

The discrepancy between fine and coarse grains and the different pattern of growth for laboratory OSL signals as function of dose apply to the Middle and Lower Danube basin loess deposits as well as to Chinese Loess Plateau deposits. This out rules the hypothesis that the quartz origin is causing this phenomenon and confirms that the discrepancy is a worldwide spread effect.

Overall, the OSL chronologies obtained for the Romanian and Serbian loess sites indicate that these sections preserve a typical Late Pleistocene succession for the Danube basin. Thus, the topmost loess layer (L1) was accumulated during the last glacial period and can be broadly correlated to the MIS 2-4 records. However, no evidence of the middle pleniglacial pedogenesis (the weakly-developed pedocomplex L1S1) was observed, in contrast to other

sections in the Vojvodina and Dobrogea region. In the case of the Orlovat section, the OSL chronology suggests that this is caused by hiatus in the sediment archive. The luminescence results also indicate that the first palaeosol (S1) identified in the investigated Danubian sites formed during the MIS 5. Additionally, for the first time to our knowledge, in SAR-OSL dating using quartz in loess deposits, for Costinești section the obtained coarse quartz chronology for the penultimate loess layer (L2) spans from ~120 ka to ~190 ka and thus does not underestimate the expected geological ages. Thus, the upper part of L2 is confidently assigned to the demise of the penultimate glacial period and can be correlated with the ending of MIS 6 in marine records.

Regarding the Xifeng site, from the central Chinese Plateau, both fine and coarse quartz assign an age of ~ 12 ka to the last glacial loess-modern soil transition and an age of ~25 ka to the transition from the weak developed palaeosol to the overlying loess. These results correlate to OSL chronologies from Luochuan loess site as well as with the marine isotope stage MIS 2/1 and MIS 3/2 boundaries. As in the case of Danube basin loess, samples older than >25 ka yield discrepant ages on different quartz grain-sizes.

Table 1 Summary of the luminescence age results on Costinești section, Dobrogea, SE Romania. All associated uncertainties represent 1σ . The associated uncertainties were calculated based on the error assessment system reported by **Aitken and Aldred (1972); Aitken (1976)**. A water content of $10 \pm 2.5\%$ was assumed over geological times. The total dose rate comprises the contribution from the alpha, beta and gamma radiations as well as the contribution of the cosmic rays. Cosmic ray contribution was derived based on the equations published by **Prescott and Hutton (1994)**. The dose rates were calculated using the conversion factors tabulated by **Adamiec and Aitken (1998)**. For fine grains the alpha efficiency factor considered was 0.04 ± 0.02 . A beta attenuation and etching factor of 0.94 ± 0.045 was considered for 63–90 μm grains (**Aitken, 1985; Appendix C**)

Sampling depth (cm)	Sample	Grain size (μm)	Equivalent dose (Gy)	U-Ra (Bq kg^{-1})	Th (Bq kg^{-1})	K (Bq kg^{-1})	Total random error (%)	Total systematic error (%)	Total dose rate (Gy ka^{-1})	Age (ka)	
L1	70	CST 1	63-90	116 ± 8 _{n=20}	33 ± 1	35 ± 2	458 ± 7	7	7	2.69 ± 0.04	43 ± 4
			4-11	90 ± 1 _{n=11}					2	8	3.19 ± 0.04
	80	CST2	63-90	129 ± 9 _{n=19}	33 ± 1	35 ± 2	445 ± 7	7	7	2.65 ± 0.04	49 ± 5
			4-11	111 ± 1 _{n=15}					1	9	3.14 ± 0.04
	90	CST3	63-90	117 ± 6 _{n=24}	31 ± 2	33 ± 1	461 ± 7	5	7	2.62 ± 0.03	45 ± 4
			4-11	105 ± 3 _{n=6}					3	8	3.09 ± 0.04
	100	CST4	63-90	157 ± 14 _{n=11}	32 ± 1	32 ± 1	419 ± 6	9	7	2.50 ± 0.02	63 ± 7
			4-11	158 ± 2 _{n=6}					2	9	2.97 ± 0.03
	110	CST5	63-90	189 ± 6 _{n=14}	30 ± 1	31 ± 1	412 ± 5	3	7	2.43 ± 0.03	78 ± 6
			4-11	173 ± 4 _{n=8}					3	9	2.88 ± 0.03
	120	CST6	63-90	205 ± 7 _{n=10}	32 ± 1	32 ± 1	416 ± 6	4	7	2.49 ± 0.03	82 ± 6
			4-11	197 ± 7 _{n=6}					4	9	2.94 ± 0.03
	130	CST7	63-90	195 ± 6 _{n=15}	31 ± 1	34 ± 1	449 ± 7	5	7	2.59 ± 0.02	79 ± 7
			4-11	196 ± 3 _{n=6}					2	9	3.07 ± 0.04
	140	CST8	63-90	250 ± 13 _{n=13}	30 ± 1	32 ± 1	453 ± 7	5	7	2.55 ± 0.03	98 ± 8
			4-11	206 ± 5 _{n=6}					2	8	3.02 ± 0.04
	150	CST9	63-90	324 ± 19 _{n=12}	33 ± 1	36 ± 1	498 ± 7	6	7	2.80 ± 0.04	116 ± 10
			4-11	269 ± 5 _{n=7}					2	8	3.29 ± 0.04
	160	CST10	63-90	296 ± 21 _{n=10}	32 ± 1	36 ± 2	480 ± 7	7	7	2.74 ± 0.04	108 ± 11
			4-11	204 ± 5 _{n=7}					2	9	3.24 ± 0.04

Table 1 (*Continuation*)

Sampling depth (cm)	Sample	Grain size (μm)	Equivalent dose (Gy)	U-Ra (Bq kg^{-1})	Th (Bq kg^{-1})	K (Bq kg^{-1})	Total random error (%)	Total systematic error (%)	Total dose rate (Gy ka^{-1})	Age (ka)	
S1	170	CST11	63-90	270 ± 27 _{n=10}	33 ± 1	40 ± 1	505 ± 7	10	7	2.88 ± 0.03	94 ± 11
			4-11	215 ± 2 _{n=7}				2	9	3.42 ± 0.04	63 ± 6
	180	CST12	63-90	334 ± 23 _{n=14}	32 ± 1	39 ± 1	518 ± 6	7	7	2.89 ± 0.02	116 ± 11
			4-11	217 ± 1 _{n=14}				2	8	3.41 ± 0.04	65 ± 6
	190	CST13	63-90	342 ± 18 _{n=14}	32 ± 2	37 ± 1	519 ± 8	5	7	2.84 ± 0.04	121 ± 10
			4-11	231 ± 2 _{n=11}				2	8	3.35 ± 0.04	70 ± 6
L2	295	CST14	63-90	480 ± 36 _{n=18}	28 ± 1	30 ± 1	458 ± 7	4	7	2.47 ± 0.03	194 ± 15
			4-11	270 ± 5 _{n=14}				3	8	2.90 ± 0.04	94 ± 8
	310	CST15	63-90	429 ± 38 _{n=18}	28 ± 1	35 ± 1	485 ± 7	8	7	2.63 ± 0.03	160 ± 17
			4-11	301 ± 4 _{n=18}				2	8	3.02 ± 0.04	100 ± 9
	330	CST16	63-90	400 ± 38 _{n=14}	29 ± 1	35 ± 1	503 ± 6	10	7	2.67 ± 0.02	150 ± 17
			4-11	314 ± 9 _{n=6}				3	8	3.15 ± 0.04	100 ± 9
	350	CST17	63-90	404 ± 33 _{n=10}	29 ± 1	33 ± 1	469 ± 7	8	7	2.54 ± 0.03	159 ± 17
			4-11	331 ± 9 _{n=5}				3	8	3.00 ± 0.04	109 ± 10
	370	CST18	63-90	425 ± 27 _{n=13}	31 ± 1	36 ± 2	520 ± 7	6	7	2.79 ± 0.03	152 ± 14
			4-11	387 ± 8 _{n=5}				2	8	3.29 ± 0.04	117 ± 10
	390	CST19	63-90	452 ± 22 _{n=10}	35 ± 1	31 ± 1	521 ± 8	5	7	2.79 ± 0.03	162 ± 14
			4-11	387 ± 12 _{n=5}				4	8	3.30 ± 0.04	118 ± 11
	410	CST20	63-90	391 ± 27 _{n=10}	33 ± 1	36 ± 1	509 ± 7	7	7	2.77 ± 0.02	141 ± 20
			4-11	410 ± 7 _{n=5}				2	8	3.28 ± 0.04	125 ± 11
	430	CST21	63-90	365 ± 48 _{n=12}	34 ± 1	40 ± 1	532 ± 8	13	7	2.92 ± 0.03	125 ± 19
			4-11	116 ± 8 _{n=20}				3	9	3.47 ± 0.04	123 ± 11
	450	CST22	63-90	90 ± 1 _{n=11}	34 ± 1	36 ± 1	551 ± 8	7	7	2.92 ± 0.03	144 ± 14
			4-11	129 ± 9 _{n=19}				2	8	3.46 ± 0.04	111 ± 10
	470	CST23	63-90	111 ± 1 _{n=15}	39 ± 1	35 ± 1	557 ± 8	10	7	3.01 ± 0.03	160 ± 20
			4-11	117 ± 6 _{n=24}				2	9	3.57 ± 0.04	116 ± 10
	490	CST24	63-90	105 ± 3 _{n=6}	36 ± 1	36 ± 2	534 ± 7	12	7	2.90 ± 0.03	190 ± 26
			4-11	157 ± 14 _{n=11}				2	9	3.45 ± 0.04	120 ± 11
	510	CST25	63-90	409 ± 12 _{n=6}	30 ± 1	38 ± 1	557 ± 8	8	7	2.88 ± 0.03	163 ± 17
			4-11	470 ± 38 _{n=13}				3	8	3.39 ± 0.04	121 ± 10

Table 2. Summary of the luminescence age results on Lunca section, SW Romania.. The assumed water content ($5 \pm 1.3\%$) over geological times was determined based on the difference between the natural “as found” and the dry weight of the material extracted from the ends of the tubes, with a relative error of 25%.

Sampling depth (cm)	Sample	Grain size (μm)	Equivalent dose (Gy)	U-Ra (Bq kg^{-1})	Th (Bq kg^{-1})	K (Bq kg^{-1})	Total random error (%)	Total systematic error (%)	Total dose rate (Gy ka^{-1})	Age (ka)
L1	LCA 1	4-11	$40 \pm 1_{n=10}$	31.1 ± 0.5	40.7 ± 0.8	479 ± 7	5	9	3.53 ± 0.15	11 ± 1
		63-90	$34 \pm 2_{n=14}$				5	7	2.98 ± 0.03	11 ± 1
	LCA 2	4-11	$65 \pm 1_{n=6}$	32.8 ± 0.8	40.4 ± 0.1	466 ± 7	4	9	3.52 ± 0.15	19 ± 2
		63-90	$58 \pm 5_{n=9}$				9	7	2.96 ± 0.03	20 ± 2
	LCA 3	4-11	$75 \pm 1_{n=4}$	33.3 ± 0.7	33.6 ± 1.3	466 ± 8	4	9	3.33 ± 0.14	22 ± 2
		63-90	$88 \pm 9_{n=7}$				10	7	2.85 ± 0.03	31 ± 4
	LCA 4	4-11	$79 \pm 1_{n=4}$	34.6 ± 0.7	39.1 ± 1.7	475 ± 8	5	9	3.57 ± 0.15	22 ± 2
		63-90	$71 \pm 5_{n=4}$				5	7	2.99 ± 0.04	24 ± 2
	LCA 5	4-11	$74 \pm 1_{n=6}$	33.6 ± 0.6	38.6 ± 1.1	498 ± 7	5	9	3.59 ± 0.15	21 ± 2
		63-90	$72 \pm 7_{n=3}$				9	7	3.03 ± 0.03	25 ± 3
	LCA 6	4-11	$76 \pm 1_{n=5}$	34.7 ± 0.4	41.3 ± 0.5	492 ± 8	5	9	3.66 ± 0.15	21 ± 2
		63-90	$67 \pm 4_{n=3}$				7	7	3.07 ± 0.03	22 ± 2
	LCA 7	4-11	$77 \pm 2_{n=8}$	32.1 ± 0.5	38.3 ± 1.6	480 ± 7	5	9	3.48 ± 0.15	22 ± 2
		63-90	$86 \pm 6_{n=14}$				11	7	2.93 ± 0.04	29 ± 3
	LCA 9	4-11	$103 \pm 10_{n=3}$	37.7 ± 0.4	41.1 ± 0.5	520 ± 7	11	9	3.82 ± 0.16	27 ± 4
		63-90	$106 \pm 6_{n=8}$				6	7	3.20 ± 0.02	33 ± 3
	LCA 11	4-11	$116 \pm 6_{n=5}$	36.7 ± 0.6	43.3 ± 1.0	529 ± 8	7	9	3.87 ± 0.16	30 ± 3
		63-90	$103 \pm 5_{n=11}$				4	7	3.24 ± 0.03	32 ± 3
	LCA 13	4-11	$117 \pm 2_{n=9}$	32.8 ± 0.7	36.4 ± 2.0	473 ± 6	5	9	3.42 ± 0.15	34 ± 3
		63-90	$114 \pm 8_{n=12}$				7	7	3.28 ± 0.03	40 ± 4
LCA 15	4-11	$113 \pm 2_{n=11}$	38.0 ± 1.0	44.8 ± 0.1	531 ± 8	5	9	3.94 ± 0.17	29 ± 3	
	63-90	$117 \pm 5_{n=17}$				5	7	3.29 ± 0.03	36 ± 3	
LCA 17	4-11	$129 \pm 2_{n=3}$	34.4 ± 0.2	43.6 ± 0.3	521 ± 8	4	9	3.78 ± 0.16	34 ± 3	
	63-90	$172 \pm 16_{n=6}$				9	7	3.17 ± 0.02	54 ± 6	

Table 2 Summary of the luminescence age results on Lunca section, SW Romania. (*Continuation.*)

Sampling depth (cm)	Sample	Grain size (μm)	Equivalent dose (Gy)	U-Ra (Bq kg^{-1})	Th (Bq kg^{-1})	K (Bq kg^{-1})	Total random error (%)	Total systematic error (%)	Total dose rate (Gy ka^{-1})	Age (ka)
241	LCA 19	4-11	$124 \pm 4_{n=7}$	34.3 ± 0.7	43.8 ± 0.4	546 ± 7	6	9	3.86 ± 0.17	32 ± 3
		63-90	$132 \pm 8_{n=13}$				6	7	3.24 ± 0.02	41 ± 4
260	LCA 21	4-11	$147 \pm 2_{n=6}$	32.9 ± 1.2	42.5 ± 0.4	495 ± 8	5	9	3.62 ± 0.15	41 ± 4
		63-90	$143 \pm 6_{n=12}$				4	7	3.04 ± 0.03	47 ± 4
278	LCA 23	4-11	$136 \pm 4_{n=5}$	33.5 ± 0.6	39.7 ± 0.8	487 ± 8	5	9	3.55 ± 0.15	38 ± 4
		63-90	$154 \pm 7_{n=7}$				5	7	2.97 ± 0.03	52 ± 4
287	LCA 24	4-11	$145 \pm 3_{n=8}$	33.2 ± 0.1	40.7 ± 0.1	483 ± 7	5	9	3.54 ± 0.15	41 ± 4
		63-90	$145 \pm 11_{n=13}$				8	7	2.95 ± 0.02	49 ± 5
295	LCA 25	4-11	$157 \pm 3_{n=6}$	33.6 ± 0.7	42.6 ± 0.5	507 ± 8	5	9	3.67 ± 0.16	43 ± 4
		63-90	$155 \pm 10_{n=10}$				7	7	3.08 ± 0.03	50 ± 5
304	LCA 26	4-11	$150 \pm 3_{n=5}$	32.6 ± 0.7	39.1 ± 0.8	523 ± 8	5	9	3.63 ± 0.16	41 ± 4
		63-90	$161 \pm 5_{n=6}$				3	7	3.05 ± 0.03	53 ± 4

Table 3. Summary of the luminescence age results on Orlovat section, Vojvodina region, Serbia. All associated uncertainties represent 1σ . The associated uncertainties were calculated based on the error assessment system reported by **Aitken and Aldred (1972)** and **Aitken (1976)**. The assumed water content over geological times was determined based on the difference between the natural “as found” and the dry weight of the material extracted from the ends of the tubes, with a relative error of 25%. For the two lowermost samples the assumed water content was 20 % and 15 % respectively, whereas for the rest of the samples it was 10%. The total dose rate comprises the contribution from the alpha, beta and gamma radiations as well as the contribution of the cosmic rays. Cosmic ray contribution was derived based on the equations published by **Prescott and Hutton (1994)**. The dose rates were calculated using the conversion factors tabulated by **Adamiec and Aitken (1998)**. For fine grains the alpha efficiency factor considered was 0.04 ± 0.02 . A beta attenuation and etching factor of 0.94 ± 0.045 was considered for 63–90 μm grains (**Aitken, 1985; Appendix C**)

Sampling depth (cm)	Sample	Grain size (μm)	Equivalent dose (Gy)	U-Ra (Bq kg^{-1})	Th (Bq kg^{-1})	K (Bq kg^{-1})	Total random error (%)	Total systematic error (%)	Total dose rate (Gy ka^{-1})	Age (ka)	
L2	965	ORL 1	4-11	292 ± 10	32.4 ± 0.9	35.6 ± 0.3	406 \pm 4	3.6	11.1	2.63 ± 0.03	111 \pm 13
			63-90	347 ± 38				11	9.2	2.18 ± 0.02	159 \pm 23
S1	700	ORL 2	4-11	196 ± 4	31.9 ± 0.6	38.6 ± 0.4	456 \pm 7	2.4	9.8	2.98 ± 0.04	66 \pm 7
			63-90	229 ± 24				10.5	7.9	2.49 ± 0.02	92 \pm 12
	600	ORL 3	4-11	182 ± 4	37.0 ± 0.6	38.2 ± 0.3	471 \pm 7	2.5	9.9	3.31 ± 0.04	55 \pm 6
			63-90	225 ± 13				5.8	7.9	2.76 ± 0.02	81 \pm 8
L1	500	ORL 4	4-11	175 ± 4	32.1 ± 0.4	36.0 ± 0.4	444 \pm 7	2.6	8.8	3.07 ± 0.04	57 \pm 5
			63-90	181 ± 10				5.6	6.7	2.57 ± 0.02	70 \pm 6
	400	ORL 5	4-11	143 ± 3	34.4 ± 0.4	37.1 ± 0.3	462 \pm 6	2.4	8.8	3.22 ± 0.04	44 \pm 4
			63-90	180 ± 10				5.6	6.7	2.70 ± 0.02	67 \pm 6
	300	ORL 6	4-11	102 ± 2	37.4 ± 0.5	42.6 ± 0.3	546 \pm 7	2.3	8.7	3.69 ± 0.04	28 \pm 3
			63-90	133 ± 7				5.3	6.7	3.10 ± 0.02	43 \pm 4
	180	ORL 7	4-11	42.0 ± 0.5	35.7 ± 0.6	34.9 ± 0.4	481 \pm 7	1.7	8.6	3.39 ± 0.04	13 \pm 1
			63-90	36.3 ± 1.8				5.0	6.6	2.78 ± 0.02	13 \pm 1
	150	ORL 8	4-11	28.2 ± 0.3	34.8 ± 0.7	35.7 ± 0.2	476 \pm 6	1.6	8.6	3.29 ± 0.04	9 \pm 1
			63-90	28.8 ± 1.1				3.9	6.6	2.77 ± 0.02	10 \pm 1

Table 4 Summary of the luminescence age results on Xifeng section, central Chinese Loess Plateau, China. All associated uncertainties represent 1σ . The associated uncertainties were calculated based on the error assessment system reported by **Aitken and Allred (1972)** and **Aitken (1976)**. A water content of $10 \pm 2.5\%$ was assumed over geological times. The total dose rate comprises the contribution from the alpha, beta and gamma radiations as well as the contribution of the cosmic rays. Cosmic ray contribution was derived based on the equations published by **Prescott and Hutton (1994)**. The dose rates were calculated using the conversion factors tabulated by **Adamiec and Aitken (1998)**. For fine grains the alpha efficiency factor considered was 0.04 ± 0.02 . A beta attenuation and etching factor of 0.94 ± 0.045 was considered for 63–90 μm grains (**Aitken, 1985; Appendix C**).

Sampling depth (m)	Sample	Grain size (μm)	Equivalent dose (Gy)	U-Ra (Bq kg^{-1})	Th (Bq kg^{-1})	K (Bq kg^{-1})	Total random error (%)	Total systematic error (%)	Total dose rate (Gy ka^{-1})	Age (ka)	
L1	1.3	XF 13	4-11	$43 \pm 1_{n=14}$	29.5 ± 1.1	39.6 ± 1.4	578 ± 9	2.46	8.18	3.55 ± 0.04	12 ± 1
		63-90	$36 \pm 2_{n=19}$	4.70				6.70	3.02 ± 0.04	12 ± 1	
	5.3	XF 53	4-11	$98 \pm 1_{n=14}$	29.2 ± 3.3	44.1 ± 1.9	674 ± 11	1.66	8.12	3.87 ± 0.05	25 ± 2
		63-90	$84 \pm 4_{n=6}$	5.60				6.80	3.29 ± 0.06	25 ± 2	
	8.3	XF 83	4-11	$159 \pm 2_{n=14}$	33.2 ± 0.4	45.7 ± 1.9	704 ± 11	1.61	8.25	4.07 ± 0.05	39 ± 3
		63-90	$162 \pm 6_{n=8}$	4.00				6.90	3.45 ± 0.04	47 ± 4	
	12.4	XF 124	4-11	$215 \pm 2_{n=15}$	31.4 ± 0.8	44.4 ± 2.6	701 ± 12	1.65	8.22	3.96 ± 0.05	54 ± 5
		63-90	$239 \pm 8_{n=13}$	3.60				6.90	3.37 ± 0.05	71 ± 6	
S1	15.3	XF 153	4-11	$280 \pm 4_{n=15}$	9.5 ± 1.4	13.2 ± 0.8	704 ± 16	2.12	6.65	2.74 ± 0.05	102 ± 7
		63-90	$234 \pm 9_{n=16}$	3.50				7.10	2.47 ± 0.05	131 ± 10	
	16.5	XF 165	4-11	$276 \pm 4_{n=15}$	30.4 ± 0.6	40.6 ± 0.8	588 ± 10	2.05	8.46	3.49 ± 0.05	79 ± 7
		63-90	$308 \pm 9_{n=15}$	3.00				6.90	2.95 ± 0.03	104 ± 8	
L2	17.5	XF 175	4-11	$332 \pm 5_{n=13}$	28.3 ± 0.4	39.4 ± 1.0	567 ± 9	1.97	8.44	3.35 ± 0.04	99 ± 9
		63-90	$241 \pm 6_{n=17}$	2.70				6.90	2.83 ± 0.03	85 ± 6	

4 Fundamental investigations into the cause of the SAR OSL age discrepancies on different grains-sizes of quartz

4.1 Quartz luminescence response to a mixed alpha-beta field

A main difference in coarse- and fine-grained quartz dating lies in the alpha irradiation history of the fine grains compared to the etched quartz grains. However, the effect of the mixed alpha-beta fields has received little attention so far. By applying time resolved optically stimulated luminescence it was confirmed that the OSL signals induced in quartz by alpha and beta radiation follow the same recombination path (data not shown).

It was investigated whether α and β laboratory irradiations designed to reproduce as closely as possible the natural irradiation field produce a different growth curve compared to only beta irradiations. As seen in **Figure 9**, the mixed alpha-beta dose response (simulating the natural contribution of the two irradiation types) reproduces the beta dose response up to about 800 Gy.

Most importantly, it was shown that the exposure of fine grains to alpha radiation during burial and transport cycles prior to deposition, as well as exposure to the mixed radiation field experienced during burial are not responsible for the age discrepancies previously reported on fine and coarse grained quartz extracted from Romanian and Serbian loess. Based on the results presented in **Figure 10**, it is unlikely that prior alpha exposure plays a significant role in affecting the shape of the subsequently measured beta dose response curves.

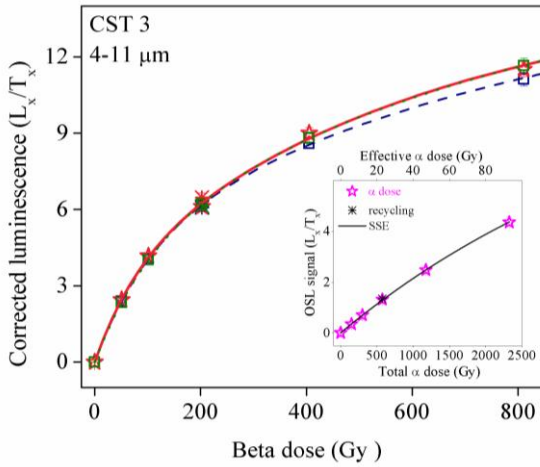


Figure 9. Mixed α - β dose response curve (solid line) normalized to a 17 Gy of beta. Each dose delivered combines a 12 % contribution of alpha and 88 % of β irradiation, to reproduce the natural radiation field experienced by sample CST 3 (6 Gy eff α + 45 Gy β , 12 Gy eff α + 90 β , 23 Gy eff α + 179 β , 47 Gy eff α + 358 β , 93 Gy eff α + 717 β). In order to better reproduce natural irradiation, doses have been delivered in mixed α/β pulses (6 Gy eff α + 45 Gy β). Pure beta growth curves were constructed before (dashed line) and after (dotted line) the mixed dose response one. The inset presents the pure alpha growth curve build on the same quartz aliquot using the alpha doses delivered in the mixed radiation experiment. Sensitivity changes were monitored using a 17 Gy beta dose.

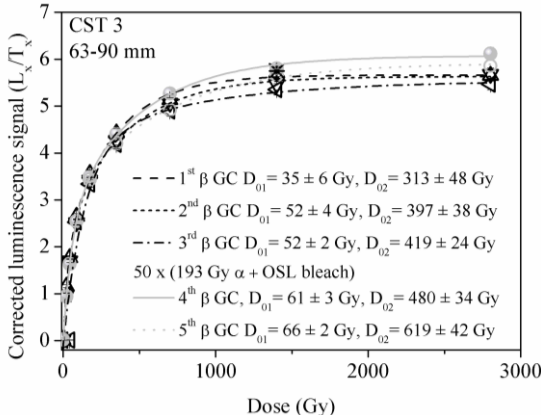


Figure 10 The effect of irradiation with a total α dose of 238.8 kGy (effective α dose of 9552 Gy assuming an a -value of 0.04) prior to the construction of the β dose response curve. The dashed lines represent the β dose response curves constructed on a single aliquot of 63-90 μm etched coarse quartz from sample CST 3 prior to alpha irradiation. The grey solid line represents β dose response constructed on the same aliquot following α irradiation. α doses were delivered in pulses of 193 Gy followed by exposure to blue LEDs for 200 s at 20 $^{\circ}\text{C}$. The dose response was best described by a sum of two exponential functions and the characteristic doses are indicated for each growth curve.

4.2 Fundamental investigations of natural and laboratory generated SAR dose response curves for quartz OSL in the high dose range

As previously reported by **Timar-Gabor et al. (2011)**, the SAR-OSL signal growth of fine as well as coarse quartz grains from Romanian samples cannot be fitted by a single saturating exponential function. Dose response curves up to full saturation were constructed on quartz extracted from several Romanian loess sites (Mircea-Vodă, Costinești, Mostiștea, Lunca and Căciulatești). Using a sum of two single saturating exponential functions to interpolate the data, the characteristic saturation parameters D_{01} and D_{02} obtained after investigating multiple aliquots are of ~140 and ~1400 Gy (fine grains) and ~65 and ~650 Gy (coarse grains) respectively (**Fig. 11**). For the Chinese quartz samples similar values for the parameters have been determined, showing the observed growth of the OSL signal with dose is inherent to quartz of different sedimentary origins (**Fig. 12**). It was shown that laboratory saturation characteristics are not affected by previous irradiation, bleaching, or the thermal treatments employed. Analysis of time resolved spectra indicated similar luminescence lifetimes for both fine and coarse quartz grains, and natural and laboratory generated OSL signals seem to use the same non-dose-dependent recombination pathways. A representative example is given in **Figure 13** on Costinești samples.

At Costinești the natural signals of a sample with an expected equivalent dose of 2000-2500 Gy were found to be below the saturation level of the laboratory dose response curve for both grain sizes. Following this observation natural dose response curves using the available information from the paleomagnetic data have been constructed and these dose response curves have been

compared to the SAR laboratory growth curves (**Fig. 14**). For doses higher than about 200 Gy natural and laboratory dose response curves for fine grains diverge, with natural signals showing earlier saturation. For 63-90 μm quartz, it was difficult to assess the degree of overlap of the natural and laboratory dose response due to the scatter of the datapoints; however, it is clear that the levels of saturation of the laboratory and natural responses are different in the case of both grain sizes. This was further confirmed for loess samples from the Lunca section (data not shown).

When signals after irradiating the samples with >8000 Gy given on top of natural doses for Romanian and Chinese quartz were measured in a SAR protocol, these were found below the laboratory saturation level. **Figure 15** presents the results obtained on a Xifeng sample.

Additional experiments demonstrate that the SAR protocol fails to accurately recover high natural (**Fig. 16**) or laboratory (**Fig. 17**) doses using Romanian and Chinese quartz, inferring that the measurement protocol is at fault when measuring not only natural but also high laboratory doses. Thus, it was recommended that adding a large dose on top of the natural and comparing the measured signal to the laboratory saturation limit should be incorporated as a standard test for evaluating the performance of the SAR protocol, especially when applications are carried out in the high dose range.

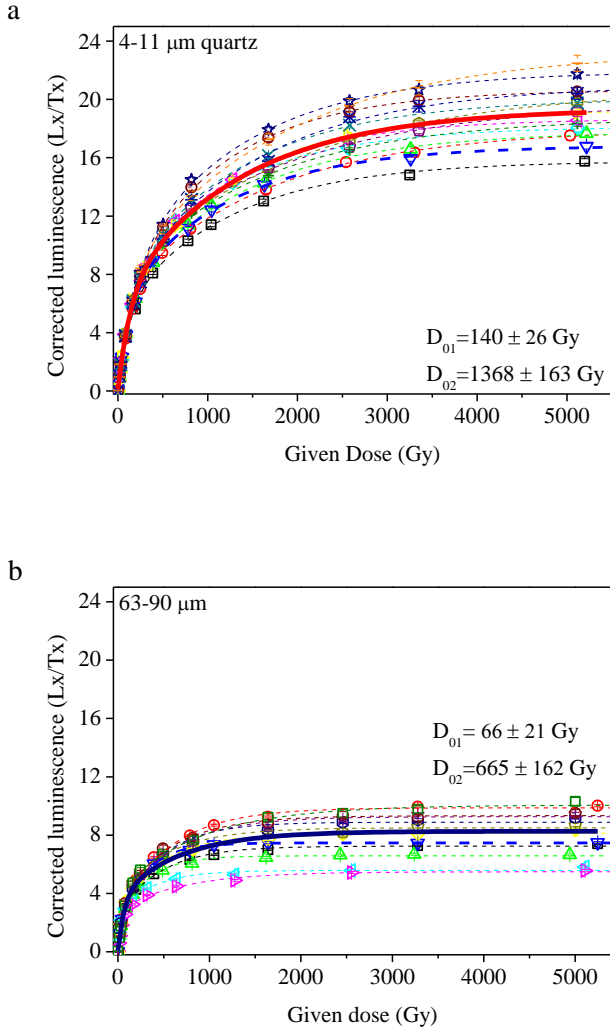


Figure 11: Laboratory dose response of (a) 15 aliquots of fine grained (4-11 μm) quartz and (b) 11 aliquots of coarse grained (63-90 μm) quartz. For fine grains, the individual values for D_{01} range between 131 ± 20 Gy and 200 ± 24 Gy, while the D_{02} values are between 1252 ± 119 Gy and 1917 ± 280 Gy. In the case of coarse grain, values for D_{01} range between 30 ± 3 Gy and 68 ± 6 Gy while the minimum and maximum values for D_{02} are 317 ± 26 Gy and 705 ± 120 Gy. The average dose response curve for each grain size is represented as a solid line.

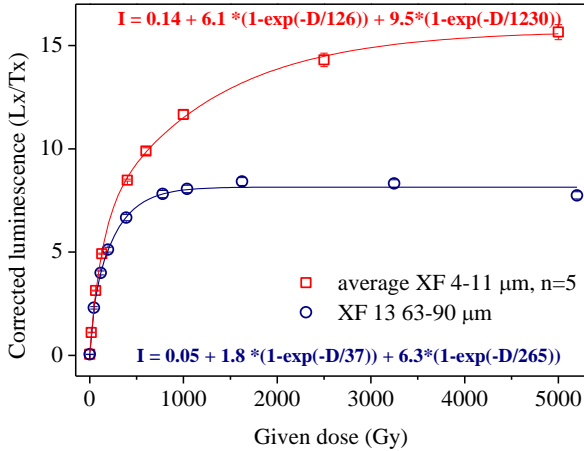


Figure 12 Average sensitivity growth curve up to 5000 Gy for fine quartz (open squares) from samples XF 83, XF 153 and XF 165 compared to a sensitivity corrected OSL signal growth curve constructed on an aliquot of coarse quartz (open circles) from sample XF 13.

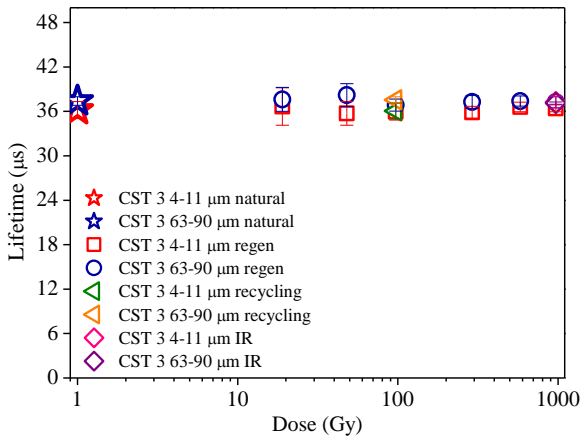


Figure 13 Average lifetimes obtained as function of dose. The lifetimes of natural signals are depicted as stars. The IR stimulation was performed in a pseudo-CW stimulation manner (on time 500 μs; off time 4.5 μs) for 100 s at 125 oC. Each datapoint represents the average value obtained on 10 aliquots.

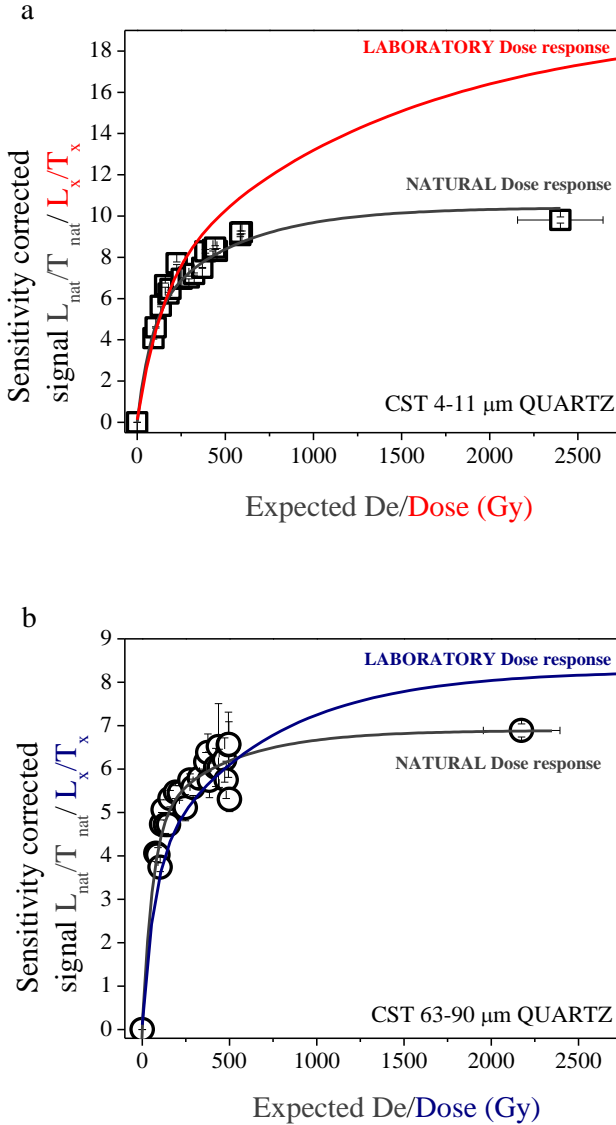


Figure 14 The average sensitivity-corrected natural signal for 26 samples from Costinești (a) fine and (b) coarse grains plotted as function of their expected equivalent dose. The average laboratory dose response curve (based on data taken up to 5000 Gy) is displayed for each grain size.

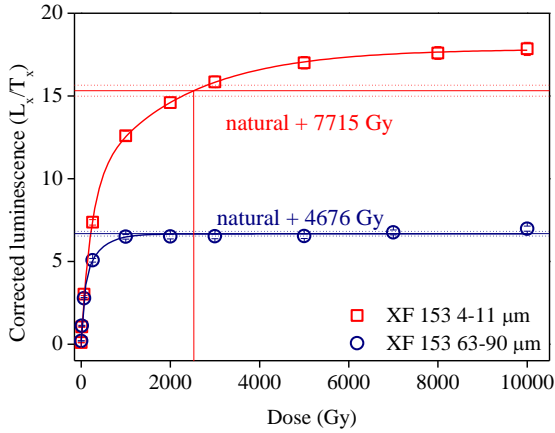


Figure 15 Normalised luminescence signals for sample XF 153 ($D_e = 280 \pm 4$ Gy- fine grains; $D_e = 324 \pm 9$ Gy- coarse grains); following irradiation to a dose of 7715 Gy for fine grains and 5120 Gy for coarse grains given on top of the natural dose. The characteristic doses for fine quartz were $D_{01} = 225 \pm 20$ Gy and $D_{02} = 2106 \pm 207$ Gy while those of coarse quartz were $D_{01} = 67 \pm 29$ Gy and $D_{02} = 357 \pm 195$ Gy.

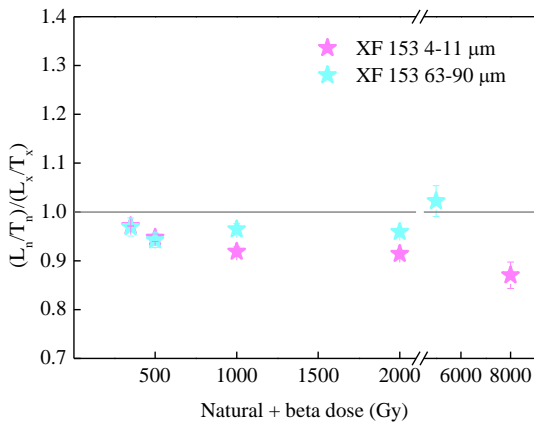


Figure 16 The SAR protocol underestimates the luminescence levels measured in the 1st measurement cycle relative to the luminescence levels induced by a regenerative dose of the same magnitude. The signals in the 1st SAR cycle correspond to the natural signals on top of which irradiation doses were given. The dashed line is meant as an eye guide for the ideal ratio.

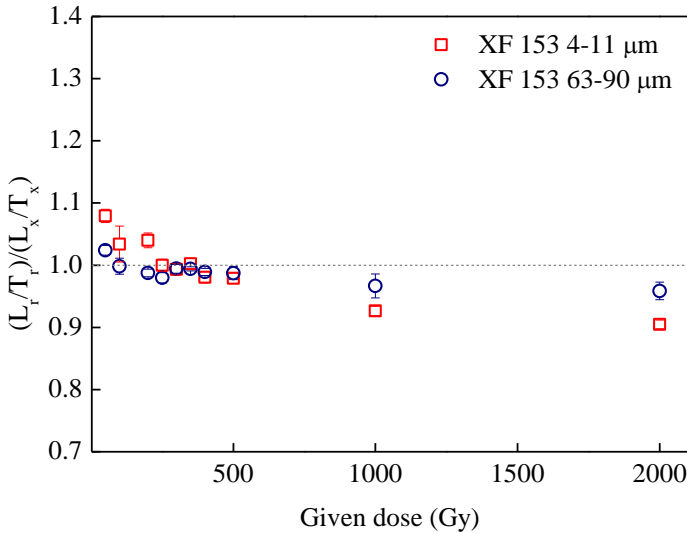


Figure 17 The SAR protocol underestimates the luminescence levels measured in the 1st measurement cycle relative to the luminescence levels induced by a regenerative dose of the same magnitude. The signals in the 1st SAR cycle are induced by irradiation doses given in the dose recovery experiments after the natural signal was reset using a double OSL bleach for 100 s at 20 °C with a 10 ks pause between them. The dashed line is meant as an eye guide for the ideal ratio.

5 Concluding remarks

At the moment, the source of the age discrepancy is thought to reside in a dose dependent phenomenon, as inferred from the different saturation characteristics of fine grains compared to the coarse grains, and the differences reported between the laboratory and the natural dose response curves. Until the mechanisms of the observed phenomena are explained and proper corrections are performed, SAR OSL ages beyond 30-40 ka can reasonably be suspected to be inaccurate. As our observations are potentially affecting

deposits worldwide, our studies raise doubts on a wealth of previous obtained chronologies.

As the age discrepancy OSL signal behaviour in quartz has been observed to be grain-size-dependent, the future experiments should employ a wider range of quartz fractions including fine material obtained through grinding or chemical etching of 63-90 μm grains. Different emissions windows should be investigated alongside the typical violet window employed routinely in quartz OSL dating studies. Deeper traps for OSL signals in quartz should be accessed. As the mechanisms giving rise to luminescence in quartz are still poorly constrained it is hoped that a future correlation of thermoluminescence (TL), optically stimulated luminescence (OSL) and electron spin resonance (ESR) investigations combined in a unitary approach will improve our level of knowledge in this respect.

References

- Adamic, G., Aitken, M., 1998. Dose-rate conversion factors: update. *Ancient TL* **16**, 37-50.
- Aitken, M., 1985. *Thermoluminescence dating*. Academic Press, London.
- Aitken, M.J., Allred, J.C., 1972. The assessment of error limits in thermoluminescent dating. *Archaeometry* **14**, 257-267.
- Aitken, M.J., 1976. Thermoluminescent age evaluation and assessment of error limits: revised system. *Archaeometry* **18**, 233-238.
- An, Z., John E., K., Warren L., P., Stefan C., P., 2001. Evolution of Asian monsoons and phased uplift of the Himalaya-Tibetan plateau since Late Miocene times. *Nature* **411**, 62-66.
- Ankjærgaard, C., Jain, M., Thomsen, K.J., Murray, A.S., 2010. Optimising the separation of quartz and feldspar optically stimulated luminescence using pulsed excitation. *Radiation Measurements* **45**, 778-785.
- Buggle, B., Glaser, B., Zöller, L., Hambach, U., Marković, S., Glaser, I., Gerasimenko, N., 2008. Geochemical characterization and origin of Southeastern and Eastern European loesses (Serbia, Romania, Ukraine). *Quaternary Science Reviews* **27**, 1058-1075.

- Buylaert, J.P., Vandenberghe, D., Murray, A.S., Huot, S., De Corte, F., Van den Haute, P., 2007. Luminescence dating of old (>70 ka) Chinese loess: A comparison of single-aliquot OSL and IRSL techniques. *Quaternary Geochronology* **2**, 9-14.
- Chapot, M.S., Roberts, H.M., Duller, G.A.T., Lai, Z.P., 2012. A comparison of natural- and laboratory-generated dose response curves for quartz optically stimulated luminescence signals from Chinese Loess. *Radiation Measurements* **47**, 1045-1052.
- Choi, J.H., Murray, A.S., Cheong, C.S., Hong, D.G., Chang, H.W., 2003. The resolution of stratigraphic inconsistency in the luminescence ages of marine terrace sediments from Korea. *Quaternary Science Reviews* **22**, 1201-1206.
- Constantin, D., Timar-Gabor, A., Veres, D., Begy, R., Cosma, C., 2012. SAR-OSL dating of different grain-sized quartz from a sedimentary section in southern Romania interbedding the Campanian Ignimbrite/Y5 ash layer. *Quaternary Geochronology* **10**, 81-86.
- Dansgaard, W., Johnsen, S.J., Clausen, H.B., Dahl-Jensen, D., Gundestrup, N.S., Hammer, C.U., Hvidberg, C.S., Steffensen, J.P., Sveinbjornsdottir, A.E., Jouzel, J., Bond, G., 1993. Evidence for general instability of past climate from a 250-kyr ice-core record. *Nature* **364**, 218-220.
- Duller, G.A.T., 2003. Distinguishing quartz and feldspar in single grain luminescence measurements. *Radiation Measurements* **37**, 161-165.
- Fan, A., Li, S.-H., Li, B., 2011. Observation of unstable fast component in OSL of quartz. *Radiation Measurements* **46**, 21-28.
- Ghenea, C., Rădan, S.C., 1993. New data on the age of loess in Dobrogea. *Romanian Journal of Stratigraphy* **75**, 133-137.
- Guo, Z.T., Peng, S.Z., Hao, Q.Z., Biscaye, P.E., Liu, T.S., 2001. Origin of the Miocene–Pliocene Red-Earth Formation at Xifeng in Northern China and implications for paleoenvironments. *Palaeogeography, Palaeoclimatology, Palaeoecology* **170**, 11-26.
- Kukla, G., 1987. Loess stratigraphy in central China. *Quaternary Science Reviews* **6**, 191-219.
- Kukla, G.J., An, Z.S., 1989. Loess stratigraphy in Central China. *Palaeogeography, Palaeoclimatology, Palaeoecology* **72**, 203–225.
- Liu, T.S., Ding, Z.L., 1998. Chinese loess and the paleomonsoon. *Annual Review of Earth and Planetary Sciences* **26**, 111-145.
- Lowick, S.E., Preusser, F., Pini, R., Ravazzi, C., 2010a. Underestimation of fine grain quartz OSL dating towards the Eemian: Comparison with palynostratigraphy from Azzano Decimo, northeastern Italy. *Quaternary Geochronology* **5**, 583-590.
- Lowick, S.E., Preusser, F., Wintle, A.G., 2010b. Investigating quartz optically stimulated luminescence dose–response curves at high doses. *Radiation Measurements* **45**, 975-984.
- Lowick, S.E., Preusser, F., 2011. Investigating age underestimation in the high dose region of optically stimulated luminescence using fine grain quartz. *Quaternary Geochronology* **6**, 33-41.

- Marković, S.B., Hambach, U., Stevens, T., Jovanović, M., O'Hara-Dhand, K., Basarin, B., Lu, H., Smalley, I., Buggle, B., Zech, M., Svirčev, Z., Sümeđi, P., Milojković, N., Zöller, L., 2012. Loess in the Vojvodina region (Northern Serbia): an essential link between European and Asian Pleistocene environments. *Netherlands Journal of Geosciences* **91**, 173-188.
- Marković, S.B., Stevens, T., Kukla, G.J., Hambach, U., Fitzsimmons, K.E., Gibbard, P., Buggle, B., Zech, M., Guo, Z., Hao, Q., Wu, H., O'Hara Dhand, K., Smalley, I.J., Újvári, G., Sümeđi, P., Timar-Gabor, A., Veres, D., Sirocko, F., Vasiljević, D.A., Jary, Z., Svensson, A., Jović, V., Lehmkuhl, F., Kovács, J., Svirčev, Z., 2015. Danube loess stratigraphy — Towards a pan-European loess stratigraphic model. *Earth-Science Reviews* **148**, 228-258.
- Martinson, D.G., Pisias, N.G., Hays, J.D., Imbrie, J., Moore, T.C., Shackleton, N.J., 1987. Age dating and the orbital theory of the ice ages: Development of a high-resolution 0 to 300,000-year chronostratigraphy. *Quaternary Research* **27**, 1-29.
- Muhs, D.R., 2007. Loess deposits, origins, and properties, In: Elias, S.A. (Ed.), *Encyclopedia of Quaternary Sciences*. Elsevier, Amsterdam, pp. 1405-1418.
- Murray, A.S., Wintle, A.G., 2000. Luminescence dating of quartz using an improved single-aliquot regenerative-dose protocol. *Radiation Measurements* **32**, 57-73.
- Murray, A.S., Wintle, A.G., 2003. The single aliquot regenerative dose protocol: potential for improvements in reliability. *Radiation Measurements* **37**, 377-381.
- Murray, A.S., Svendsen, J.I., Mangerud, J., Astakhov, V.I., 2007. Testing the accuracy of quartz OSL dating using a known-age Eemian site on the river Sula, northern Russia. *Quaternary Geochronology* **2**, 102-109.
- Necula, C., 2006. Rockmagnetic properties of loess-paleosol deposits from Romania: paleoclimatic implications. Phd Thesis, . *Fizica Atmosferei si a Globului Terestru*. University of Bucharest, Bucharest.
- Pawley, S.M., Toms, P., Armitage, S.J., Rose, J., 2010. Quartz luminescence dating of Anglian Stage (MIS 12) fluvial sediments: Comparison of SAR age estimates to the terrace chronology of the Middle Thames valley, UK. *Quaternary Geochronology* **5**, 569-582.
- Prescott, J.R., Hutton, J.T., 1994. Cosmic ray contributions to dose rates for luminescence and ESR dating: large depths and long-term time variations. *Radiation Measurements* **23**, 497-500.
- Rasmussen, S.O., Bigler, M., Blockley, S.P., Blunier, T., Buchardt, S.L., Clausen, H.B., Cvijanovic, I., Dahl-Jensen, D., Johnsen, S.J., Fischer, H., Gkinis, V., Guillevic, M., Hoek, W.Z., Lowe, J.J., Pedro, J.B., Popp, T., Seierstad, I.K., Steffensen, J.P., Svensson, A.M., Vallelonga, P., Vinther, B.M., Walker, M.J.C., Wheatley, J.J., Winstrup, M., 2014. A stratigraphic framework for abrupt climatic changes during the Last Glacial period based on three synchronized Greenland ice-core records: refining and extending the INTIMATE event stratigraphy. *Quaternary Science Reviews* **106**, 14-28.
- Rees-Jones, J., 1995. Optical dating of young sediments using fine-grain quartz. *Ancient TL* **13**, 9-14.

- Steffen, D., Preusser, F., Schlunegger, F., 2009. OSL quartz age underestimation due to unstable signal components. *Quaternary Geochronology* **4**, 353-362.
- Stevens, T., Armitage, S.J., Lu, H., Thomas, D.S.G., 2007. Examining the potential of high sampling resolution OSL dating of Chinese loess. *Quaternary Geochronology* **2**, 15-22.
- Stevens, T., Marković, S.B., Zech, M., Hambach, U., Sümeği, P., 2011. Dust deposition and climate in the Carpathian Basin over an independently dated last glacial–interglacial cycle. *Quaternary Science Reviews* **30**, 662-681.
- Stevens, T., Armitage, SJ, Lu, H, Thomas, DSG, 2006. Sedimentation and diagenesis of Chinese loess: implications for the preservation of continuous, high-resolution climate records. *Geology* **34**, 849-852.
- Svensson, A., Andersen, K. K., Bigler, M., Clausen, H. B., Dahl-Jensen, D., Davies, S. M., Johnsen, S. J., Muscheler, R., Parrenin, F., Rasmussen, S. O., Röthlisberger, R., Seierstad, I., Steffensen, J. P., Vinther, B. M., 2008. A 60 000 year Greenland stratigraphic ice core chronology. *Climate of the Past* **4**, 47-57.
- Timar-Gabor, A., Vandenberghe, D.A.G., Vasiliniuc, S., Panaiotu, C.E., Panaiotu, C.G., Dimofte, D., Cosma, C., 2011. Optical dating of Romanian loess: A comparison between silt-sized and sand-sized quartz. *Quaternary International* **240**, 62-70.
- Timar-Gabor, A., Vasiliniuc, Ş., Vandenberghe, D.A.G., Cosma, C., Wintle, A.G., 2012. Investigations into the reliability of SAR-OSL equivalent doses obtained for quartz samples displaying dose response curves with more than one component. *Radiation Measurements* **47**, 740-745.
- Timar, A., Vandenberghe, D., Panaiotu, E.C., Panaiotu, C.G., Necula, C., Cosma, C., van den haute, P., 2010. Optical dating of Romanian loess using fine-grained quartz. *Quaternary Geochronology* **5**, 143-148.
- Wintle, A.G., Murray, A.S., 2006. A review of quartz optically stimulated luminescence characteristics and their relevance in single-aliquot regeneration dating protocols. *Radiation Measurements* **41**, 369-391.
- Wintle, A.G., 2008. Luminescence dating: where it has been and where it is going. *Boreas* **37**, 471-482.